nature plants

ARTICLES

https://doi.org/10.1038/s41477-020-0645-z

Check for updates

GOLVEN peptide signalling through RGI receptors and MPK6 restricts asymmetric cell division during lateral root initiation

Ana I. Fernandez[1,2,8], Nick Vangheluwe[1,2,8], Ke Xu[1,2], Joris Jourquin[1,2], Lucas Alves Neubus Claus[1,2], Stefania Morales-Herrera[1,2,3,4], Boris Parizot[1,2], Hugues De Gernier[1,2], Qiaozhi Yu[1,2], Andrzej Drozdzecki[1,2], Takanori Maruta[5], Kurt Hoogewijs[6], Willem Vannecke[6], Brenda Peterson[7], Davy Opdenacker[1,2], Annemieke Madder[6], Zachary L. Nimchuk[7], Eugenia Russinova[1,2] and Tom Beeckman[1,2] ✉

During lateral root initiation, lateral root founder cells undergo asymmetric cell divisions that generate daughter cells with different sizes and fates, a prerequisite for correct primordium organogenesis. An excess of the GLV6/RGF8 peptide disrupts these initial asymmetric cell divisions, resulting in more symmetric divisions and the failure to achieve lateral root organogenesis. Here, we show that loss-of-function *GLV6* and its homologue *GLV10* increase asymmetric cell divisions during lateral root initiation, and we identified three members of the RGF1 INSENSITIVE/RGF1 receptor subfamily as likely GLV receptors in this process. Through a suppressor screen, we found that MITOGEN-ACTIVATED PROTEIN KINASE6 is a downstream regulator of the GLV pathway. Our data indicate that GLV6 and GLV10 act as inhibitors of asymmetric cell divisions and signal through RGF1 INSENSITIVE receptors and MITOGEN-ACTIVATED PROTEIN KINASE6 to restrict the number of initial asymmetric cell divisions that take place during lateral root initiation.

Root branching is a major determinant of root system architecture. The de novo formation of lateral roots (LRs) is a trade-off for plants to compensate for their lack of mobility while still being able to search for water and nutrients in the soil. In *Arabidopsis*, LRs arise from a subset of stem cells situated in the pericycle at the xylem poles. These cells are termed LR founder cells and undergo a series of tightly coordinated cell divisions in the differentiation zone of the root to generate cell diversity and tissue patterns, resulting in the development of an LR primordium that eventually emerges from the main root body. LR formation follows a regular spacing pattern, indicating that not all xylem-pole pericycle cells become LR founder cells and start dividing. The details of LR spacing are not well understood. Since the whole LR formation process comprises several steps, with the first steps taking place when xylem-pole pericycle cells leave the root apical meristem, each of these constitutes a regulatory check-up point for the root to adapt the number of eventually emerged LRs (ELRs).

The first event currently associated with LR formation takes place in the elongation zone of the root, where an oscillatory gene transcription mechanism is proposed to prime some xylem-pole pericycle cells before they reach the differentiation zone[1,2]. On the basis of the oscillation frequency of the *DR5pro:Luciferase* marker reporting the auxin transcriptional response, it is thought that a higher number of xylem-pole pericycle cells undergo priming than the ones that later participate in the formation of an LR. Furthermore, several genetic studies have reported on the occurrence of clustered or at least closely spaced LR primordia in mutants affected in various regulatory genes[3–6]. The oversupply of such mutants with more and closely formed LRs argues for the existence of inhibitory mechanisms that are required to restrain the division activity of the xylem-pole pericycle cells. However, the spacing of LRs can be fostered by the type of division. During the so-called LR initiation process, the nuclei of adjacent LR founder cells (which are arranged as pairs in two or three contiguous cell files) move towards the common cell wall, and both cells undergo one or two rounds of asymmetric division with an anticlinal orientation, yielding smaller central daughter cells flanked by larger ones[3,5,7]. The outcome of the asymmetric divisions is a focused centre of cell division activity in the small daughter cells surrounded by larger flanking cells that are dividing less or not dividing. The initial anticlinal divisions generate a recognizable hallmark that is referred to as a stage I primordium. Subsequent anticlinal and periclinal divisions generate a dome-shaped primordium that eventually becomes an LR[8,9].

Apart from some components of the auxin signalling cascade and the LATERAL ORGAN BOUNDARIES DOMAIN16 (LBD16) transcription factor, not many elements have been identified that regulate the LR initiation step. Recently, the GOLVEN/ROOT GROWTH FACTOR/CLE-like (GLV/RGF/CLEL) signalling peptide family has been implicated in the LR initiation process[10–12]. One of its family members, GLV6/RGF8/CLEL2 (hereafter referred to as GLV6), is transcribed in LR founder cells during nuclear migration, which reflects the repolarization of LR founder cells preparing for asymmetric cell division (ACD). *GLV6* overexpression ($GLV6^{OE}$) disturbs the initial ACD, resulting in more symmetric, seemingly

[1]Department of Plant Biotechnology and Bioinformatics, Ghent University, Ghent, Belgium. [2]VIB Center for Plant Systems Biology, Ghent, Belgium. [3]Laboratory of Molecular Cell Biology, KU Leuven, Kasteelpark, Leuven, Belgium. [4]VIB Center for Microbiology, Kasteelpark, Leuven, Belgium. [5]Department of Life Science and Biotechnology, Faculty of Life and Environmental Science, Shimane University, Matsue, Japan. [6]Department of Organic Chemistry and Macromolecular Chemistry, Ghent University, Ghent, Belgium. [7]Department of Biology, University of North Carolina, Chapel Hill, NC, USA. [8]These authors contributed equally: Ana I. Fernandez, Nick Vangheluwe. ✉e-mail: tobee@psb.ugent.be

non-formative divisions since a dome-shaped primordium is rarely formed in *GLV6*^{OE} roots. Consequently, *GLV6*^{OE} primary roots appear naked, without ELRs. Here we show that loss-of-function (*lof*) *GLV6* and its homologue *GLV10* result in increased ACDs during LR initiation. We provide evidence that GLV6/10 signalling probably involves perception by RGF1 INSENSITIVE (RGI)/RGF1 receptors (RGFR) and were able to identify MITOGEN-ACTIVATED PROTEIN KINASE6 (MPK6) as a component of the immediate downstream signalling. We propose a model of how secreted GLV peptides may restrict initial ACDs taking place during LR initiation.

Results

The GLV signalling pathway inhibits LR initiation. Our previous work demonstrated the involvement of GLV6 in LR initiation; however, in the absence of knockout mutants, a defined role could not be delineated[12]. To further corroborate the GLV6 function in LR initiation, we generated *GLV6* mutants using the CRISPR–Cas9 system. We obtained three mutant lines (*CRISPR glv6-1*, *glv6-2* and *glv6-3*) where insertions, deletions and/or gene rearrangements led to frame shifts and premature stop codons (Supplementary Table 1). The remaining sequences are predicted to encode truncated proteins of 55, 37 and 106 amino acids in the *CRISPR glv6-1*, *glv6-2* and *glv6-3* mutants, respectively, instead of the 123 amino acids normally encoded by the wild-type *GLV6* gene (Supplementary Table 1). Phenotyping of these lines revealed that only *CRISPR glv6-1* had a small increase in root length, a phenotype probably intrinsic to this line and not the consequence of *GLV6* knockout. No other difference from the wild type was observed in these mutants in either primary root length or LR density (Extended Data Fig. 1a–c and Supplementary Table 2).

In contrast to the strong *GLV6* overexpression phenotype[12], mutating *GLV6* had no effect on root system architecture, pointing to redundancy with other *GLV* genes. From our previous studies, we know that *GLV10* is expressed during early LR formation[11], suggesting redundancy with *GLV6*. In agreement with this hypothesis, *GLV10* overexpression resulted in a similar LR phenotype as *GLV6* (ref. [11]). A more detailed investigation of the *GLV10pro:nls-2XGFP* transcriptional reporter revealed low *GLV10* expression at the early stages of primordium formation, including in LR founder cells before the first division. After the first ACD and throughout development, *GLV10* transcription was strongest in the central cells (Fig. 1a). To investigate whether GLV6 and GLV10 are functionally redundant, we analysed an available sextuple *GLV* mutant generated by CRISPR–Cas9, in which *GLV6* and *GLV10*, as well as other *GLV* genes not transcribed in the root or transcribed at later LR developmental stages, were targeted (hereafter *CRISPR glv*; see Methods)[13]. No difference in the primary root length was observed in this mutant compared with the wild type (Fig. 1b and Extended Data Fig. 1d). However, in contrast to the *CRISPR glv6* mutants, an increase in the total LR density was observed, mostly owing to an accumulation of non-emerged primordia, especially at stage I (Fig. 1c,d and Supplementary Table 2). To confirm that *GLV6* and *GLV10* are responsible for the observed phenotype, we generated a *glv6 glv10* double mutant by crossing a *glv10* transfer DNA (tDNA) *lof* mutant with the *CRISPR glv6-2* mutant. The analysis of the LR phenotype revealed a small non-significant increase in total LR density in the single *glv10* mutant that was further enhanced in the *glv6 glv10* double mutant (Fig. 1e). Similar to the *CRISPR glv* mutant, non-emerged primordia, mainly at stage I, accumulated in *glv6 glv10* seedlings (Fig. 1e and Extended Data Fig. 1e). Interestingly, the observed phenotype could be complemented by growing the mutants on low concentrations of GLV6 peptide (GLV6p) or GLV10p, indicating that the phenotype reflects the lack of GLV signalling (Fig. 1c–e and Extended Data Fig. 1e). These data indicate that on *GLV6/10* knockout more pericycle cells undergo ACD, giving rise to stage I primordia, which points to a role for GLV peptides as negative regulators of LR initiation. The *glv6 glv10* phenotype was somewhat weaker than the *CRISPR glv* mutant, suggesting that other *GLV* genes targeted in the latter (for example, *GLV7*) are expressed in LR founder cells at undetectable levels in the wild type or on knocking out *GLV6* and *GLV10*.

During the formation of a stage I primordium, one or two anticlinal ACD events can take place in the central pericycle cell file[9,12] before the division plane changes to produce a two-layered primordium. After the first ACD, four cells are generated (two central short and two larger flanking cells). When a second round of ACD takes place, five or six cells are produced depending on whether one or both flanking cells underwent division (Fig. 1f). To understand whether GLV signalling is involved in inhibiting only the first or also the subsequent ACD events, we quantified the frequency of four- or five/six-celled stage I primordia. First, we observed that many of the stage I primordia were present in the mature region of the root where other primordia had developed into more advanced stages, indicating that they may be arrested (20 out of 29 (69%) in the wild type and 33 out of 51 (65%) in the *CRISPR glv* mutant). Around two-thirds of the total stage I primordia in the wild type had gone through the first ACD only, while one-third proceeded with the second one (Fig. 1g). These data suggest that not all wild-type primordia that underwent the first ACD will by default continue through the second one and point to the existence of potential checkpoints at the transition between these two events, as well as after the second ACD. Regardless of the fact that a similar proportion of stage I primordia seemed arrested in the *CRISPR glv* mutant as in the wild type, the quantification of stage I primordium cell numbers showed that the second ACD happened much more often in the *CRISPR glv* mutant, which was further confirmed in the *glv6 glv10* double mutant (Fig. 1g). These data indicate that GLV signalling may negatively regulate not only the occurrence of the first ACD, but also the transition from the first to the second ACD.

We also observed that occasionally two primordia or LRs formed in close proximity in the *glv* mutant seedlings (Fig. 1h and Extended Data Fig. 1f). Indeed, the frequency of such events was higher in the *CRISPR glv* and the *glv6 glv10* mutants than in the wild type, suggesting extra initiation sites and/or disturbed LR initiation spacing in the mutants. Once again, this phenotype was complemented by supplementing GLV6p or GLV10p to the growth medium (Fig. 1i). Altogether, the analysis of gain- and loss-of-function phenotypes points towards a function for both GLV6p and GLV10p in the control of LR initiation events during the first and second ACD steps.

Identification of downstream effectors of the GLV pathway. To better understand GLV signalling during LR initiation, we decided to search for downstream elements of the pathway. For this purpose, a suppressor screening was carried out taking advantage of the lack of visible LRs in *GLV6*^{OE} seedlings. We generated an estradiol-inducible *GLV6*^{OE} line (*iGLV6*), which offers the possibility to score mutant phenotypes in both the presence (induced) and absence (non-induced) of *GLV6* overexpression. We confirmed the inducibility of the *GLV6* transcript in the *iGLV6* line and its capability in phenocopying the constitutive *GLV6*^{OE} in the presence of estradiol, while having a wild-type phenotype in non-induced conditions (Fig. 2a–c and Supplementary Fig. 1a,b). Indeed, in the presence of estradiol, initiation events consisting of excessive anticlinal divisions were observed in the pericycle along the whole root, resulting in very few dome-shaped primordia and ELRs (Fig. 2b,c)[12]. An ethylmethane sulfonate (EMS) mutagenesis was then performed, and *iGLV6* seedlings were screened on estradiol for the presence of LRs, indicating the suppression of the *GLV6*^{OE} phenotype (Supplementary Fig 1c). We eventually obtained five confirmed mutants and named them *suppressors of GLV6*^{OE} *phenotype* (*sgps*) (Fig. 2d and Supplementary Fig. 1d).

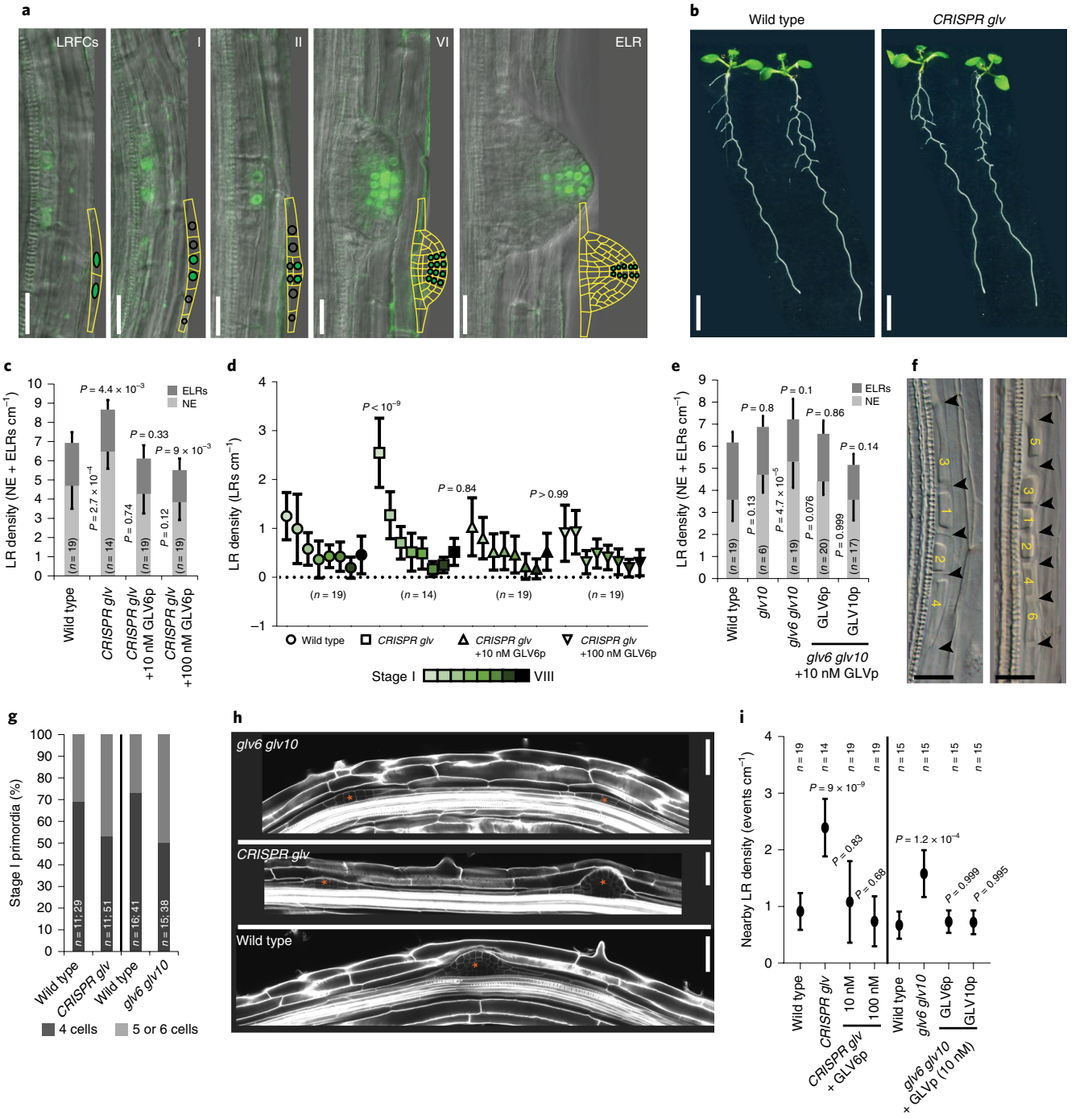

Fig. 1 | *CRISPR glv* lines have defects in LR initiation. a, *GLV10pro:nls-2XGFP* signal in LR founder cells and the forming primordium. The representative primordium stages (roman numerals indicated on the upper right side) are shown. Note that the LR founder cells (LRFCs) can be recognized by the oval shape of the nuclei. After division, the nuclei become round. Insets: representations of *GLV10* expression (green filled circles) at the different primordium stages. The empty circles indicate no *GLV10* expression in those cells (omitted at later stages). **b**, *CRISPR glv* seedlings show similar root lengths to the wild type. **c**, Quantification of non-emerged primordia (NE), ELRs and total LR density in the *CRISPR glv* mutant (8 d after germination (dag)). Significant differences from the wild type are shown for NE and total LR density. **d**, Quantification of the densities of all primordium stages in *CRISPR glv* seedlings germinated on MS medium or on GLV6p at the indicated concentrations (8 dag). **e**, Quantification of NE, ELRs and total LR density in the *glv6 glv10* mutant (8 dag) supplemented or not with GLV6p or GLV10p. Significant differences from the wild type are shown for NE and total LR density. **f**, Stage I primordia with one (left) or two (right) rounds of ACDs. The arrowheads indicate the cell borders following ACDs; the resulting daughter cells are numbered. **g**, Quantification of stage I primordia with one or two rounds of ACDs. The percentages of four- or five/six-celled stage I primordia are shown (*n*, number of roots; number of primordia). **h**, Primordia (indicated by red asterisks) are often observed in close proximity in the *CRISPR glv* and *glv6 glv10* mutants. **i**, Density of nearby LRs in *glv* mutants supplemented or not with GLV6p or GLV10p compared with the wild type. The comparisons of all genotypes and treatments with the wild type were done using a generalized estimation equations (GEE) model (**c**–**e**,**i**). See Methods for details and Supplementary Table 2 for the full statistical analysis. The charts (**c**–**e**,**i**) represent the mean values ± s.d. The scale bars represent 20 µm in **a** and **f**, 0.5 cm in **b** and 50 µm in **h**. The representative images in **a** and **b** were observed at least twice with similar results.

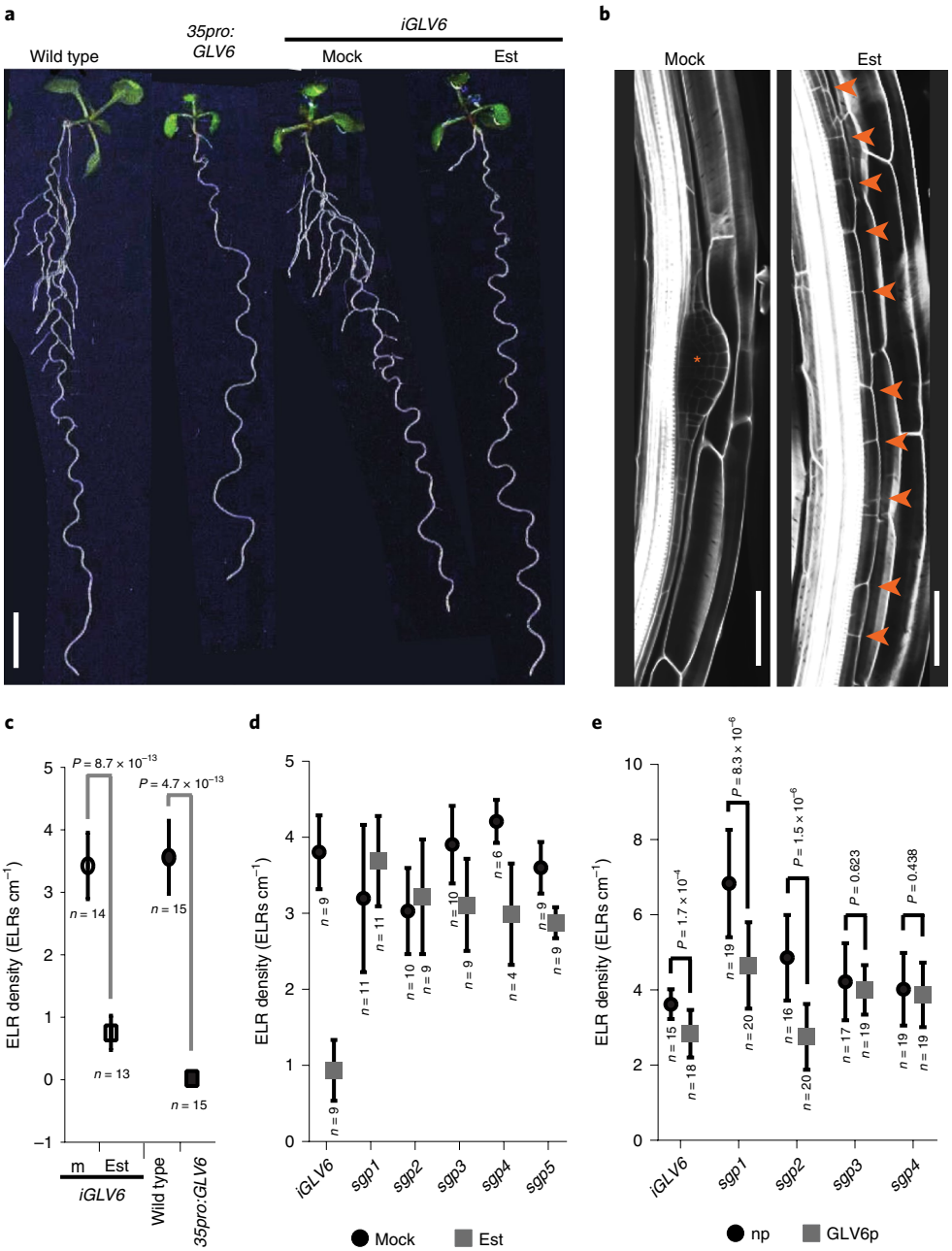

Fig. 2 | Identification of downstream components of GLV signalling during LR initiation. a–c, Phenotypical analysis of an estradiol-inducible line (*iGLV6*) that phenocopies constitutive *GLV6*^{OE}. **a**, Phenotype of *iGLV6* 13 dag seedlings in induced (2 µM estradiol) and non-induced (mock) conditions compared with constitutive *GLV6*^{OE} (*35pro:GLV6*). **b**, Ectopic anticlinal divisions (indicated by arrowheads) or normal primordium development (indicated by a red asterisk) in the pericycle of *iGLV6* roots in the presence or absence of estradiol, respectively. **c**, Quantification of ELR density in *iGLV6* and *35pro:GLV6* 13 dag seedlings compared with the controls. **d**, ELR density in confirmed 12 dag M3 mutants germinated on estradiol or mock treatments. **e**, ELR density of *sgp1-4* germinated in liquid medium supplemented or not with GLV6p (2 µM). Est, estradiol; m, mock; np, no peptide treatment. The charts (**c–e**) represent the mean values ± s.d. Different treatments for the same genotype are compared using a two-sided Student's *t*-test. The scale bars represent 0.5 cm in **a** and 50 µm in **b**.

We previously reported that treatments with the GLV6p phenocopy the ectopic pericycle divisions observed in *GLV6*^{OE} (ref. [12]). Surprisingly, *sgp1* and *sgp2* responded to GLV6p treatment, prompting us to postulate that the mutated gene was involved in the production of bioactive mature GLV peptides (Fig. 2e). Additionally, *sgp1* and *sgp2* showed similar root phenotypes as reported for the *tpst-1* mutant (Supplementary Fig. 2a,b)[14,15]. The tyrosylprotein sulphotransferase enzyme (TPST) catalyses tyrosine sulfonation in plants and is encoded by a single-copy gene in *Arabidopsis*. Tyrosine sulfonation is crucial for RGF/GLV peptide bioactivity[16,17], and accordingly, *tpst-1* mutant root phenotypes have been ascribed to a defect in the production of GLV/RGF, as well as phytosulfokine bioactive peptides. Indeed, sequencing of the *TPST* gene revealed mutations resulting in a E^{146} to K^{146} change in *sgp1*, and in a R^{195} to W^{195} change in *sgp2* (Supplementary Fig. 2c). F1 crosses of *sgp1* with *sgp2*, as well as with *tpst-1*, confirmed that they are indeed allelic (Supplementary Figs. 1e and 2d and Supplementary Table 3). We renamed *sgp1* and *sgp2* as *tpst-3* and *tpst-4*, following the

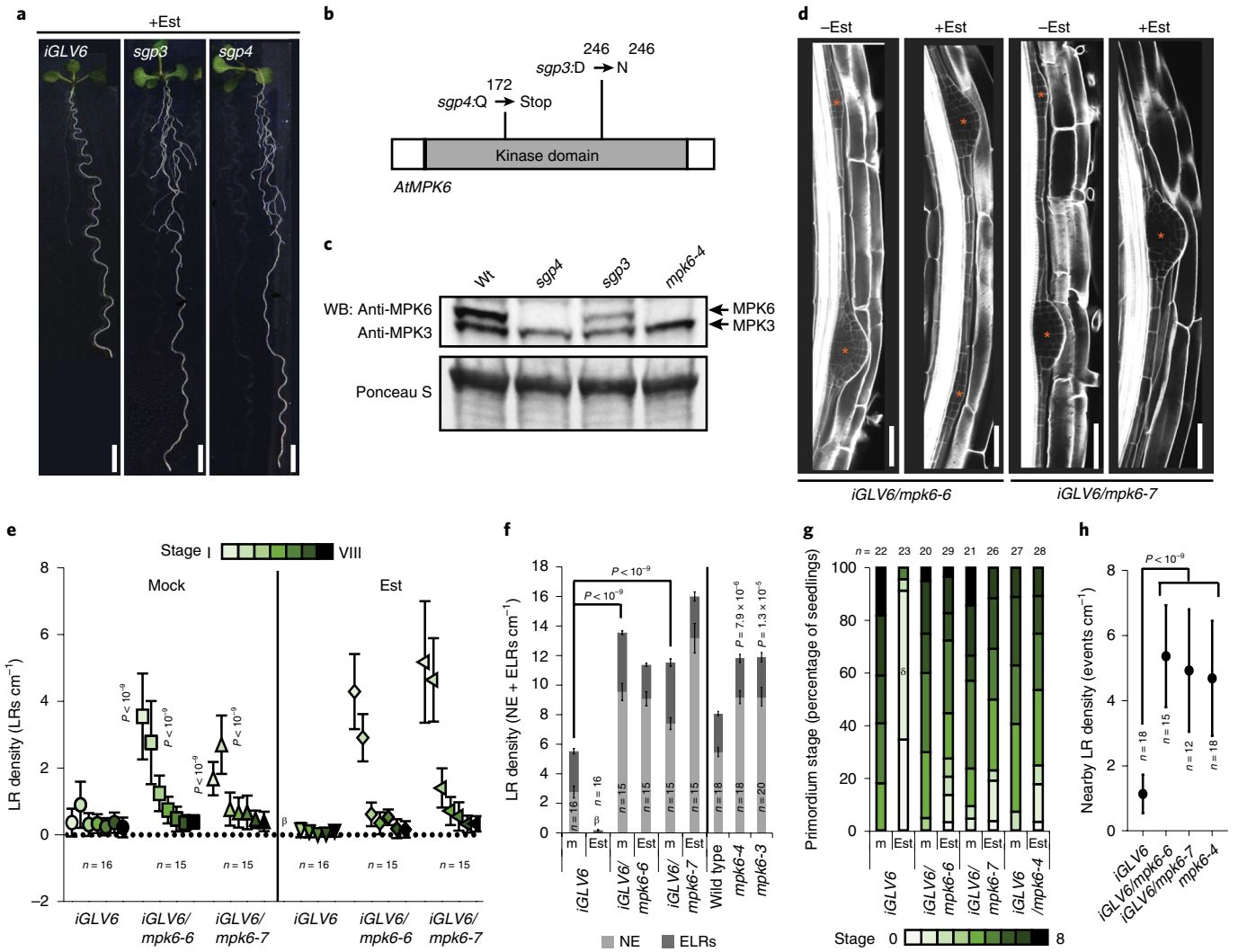

Fig. 3 | *mpk6* mutants suppress the LR *GLV6*^{OE} phenotype. a, ELRs are restored in *sgp3* and *sgp4*. **b**, Position of the respective mutations of *sgp3* and *sgp4* in the *MPK6* gene. **c**, Analysis of MPK3 and MPK6 proteins in extracts of the *sgp3* and *sgp4* mutants using anti-MPK6/MPK3 antibodies in western blots (WB). Extracts from the wild type (Wt) and *mpk6-4* are included as controls. **d**, Dome-shaped primordia are observed in *mpk6* mutants with or without estradiol. Note the primordia (indicated by red asterisks) initiating in close proximity. **e**, Quantification of all primordium stages in *iGLV6/mpk6-6* and *iGLV6/mpk6-7* with and without estradiol (8 dag). Significant differences from the wild type in stage I and II primordia under mock conditions are shown. **f**, Quantification of NE, ELRs and total LR density in the *iGLV6/mpk6-6* and *iGLV6/mpk6-7* mutants with and without estradiol, and in *mpk6* tDNA mutants germinated on MS compared with the controls (8 dag). The *P* values correspond to the analysis of total LR density. **g**, Quantification of primordia (stages) formed after primary root bending. Stages from 0 to 8 are colour-coded. Stage 0 indicates no primordia formed at the bend. **h**, Quantification of nearby primordia in *mpk6* mutants without estradiol (8 dag). No significant differences were found between different *mpk6* mutants ($0.5 < P < 1$). The charts represent the mean values ± s.d. (**e**,**h**) or s.e.m. (**f**). A GEE model was used for comparison (**e**,**f**,**h**). For the full statistical analysis, see Supplementary Table 2. For lines marked with β, wild-type-like stage I and II primordia cannot be distinguished; only anticlinally divided pericycle cells were observed, preventing the quantification of individual primordia stages. For lines marked with δ, stage I or II refers to one- or two-layered anticlinally dividing pericycles. The scale bars represent 0.5 cm in **a** and 50 µm in **d**.

nomenclature for previously reported *tpst* mutants[18]. The finding of *tpst* alleles validates the suitability of our screening strategy for identifying genes involved in the GLV signalling pathway.

In contrast to *sgp1* and *sgp2*, *sgp3* and *sgp4* suppressed the LR phenotype caused by *GLV6*^{OE} as well as peptide treatment, indicating that the mutated gene acts at the level or downstream of peptide ligand perception (Figs. 2d,e and 3a). Back-crossing *sgp3* and *sgp4* to the parental *iGLV6* line, as well as with each other, showed that the mutants are recessive and allelic with regard to the suppression of the *GLV6*^{OE} LR phenotype (Supplementary Fig. 1e and Supplementary Table 3). Next-generation sequencing revealed that both *sgp3* and *sgp4* carried mutations in the *MPK6* gene resulting in a change of a conserved amino acid in *sgp3* and in a premature stop codon in *sgp4* (Fig. 3b and Supplementary Fig. 3b). We confirmed the absence of signal in *sgp4*, while full-length MPK6 was detected in *sgp3*, probing with anti-MPK6 antibodies (Fig. 3c). Additionally, *sgp3* and *sgp4*, and F1 seedlings resulting from crossing them to the *mpk6-4* tDNA line, displayed pleiotropic root phenotypes reported earlier for *mpk6* mutants[19]. Furthermore, an *iGLV6/mpk6-4* line showed suppression of the LR root phenotype after the estradiol induction of *GLV6*^{OE} (Supplementary Fig. 3b–e). The mutants *sgp3* and *sgp4* will therefore be referred to as *iGLV6/mpk6-6* and *iGLV6/mpk6-7*, respectively. The *sgp5* mutant was also analysed using next-generation sequencing, but the

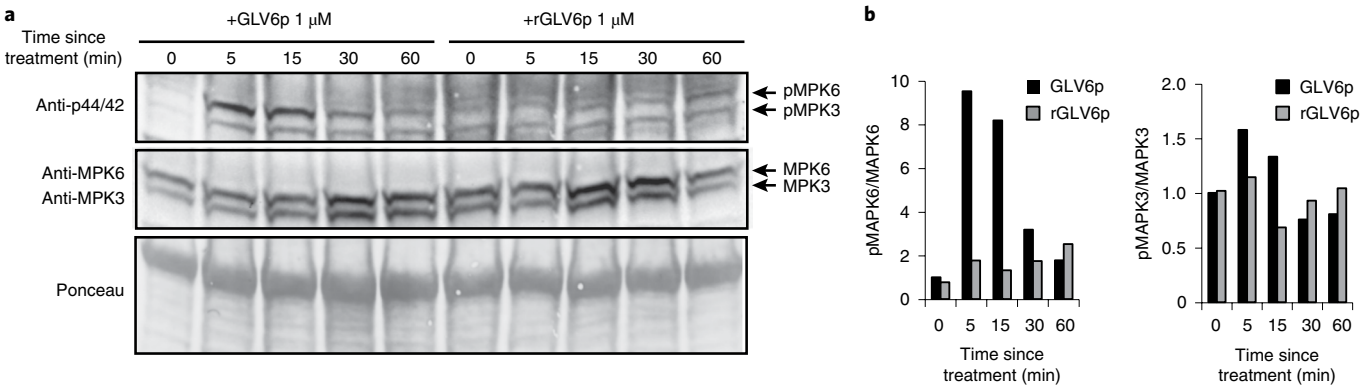

Fig. 4 | MPK6 phosphorylation is induced shortly after GLV6p treatment. a, Analysis of MPK3 and MPK6 phosphorylation and protein levels in extracts of seedlings treated with GLV6p or rGLV6p for the indicated time points. The representative western blot was probed with anti-phospho-44/42 or anti-MPK6/anti-MPK3 antibodies, and Ponceau staining was used as the loading control. Note that MPK6/MPK3 phosphorylation is specific, as rGLV6p (with the same amino acid composition as GLV6p but with a randomized sequence) did not induce protein phosphorylation. **b**, Quantification of the ratio between the phosphorylated MPK6 or MPK3 (pMPK6 or pMPK63) and the MPK6 or MPK3 protein signal shown in **a**, respectively. The fold change relative to time 0 (GLV6p) is shown. This experiment was done three times with similar results.

causative mutation for its suppression phenotype could not be demonstrated yet.

***GLV6*^{OE} ectopic anticlinal pericycle divisions are suppressed in *mpk6* mutants.** Mitogen-activated protein kinase cascades are highly conserved signalling modules downstream of peptide and receptor pairs[20]. We therefore focused on the study of MPK6 as a likely downstream effector of the GLV signalling pathway in LR initiation.

We first analysed the occurrence of excessive pericycle anticlinal divisions, typically found when *GLV6* is overexpressed, in *iGLV6/mpk6-6* and *iGLV6/mpk6-7* mutants germinated on estradiol. This analysis revealed none or very few of these divisions in the presence of estradiol in the mutants. Instead, normal primordia were formed similar to those found under non-induced conditions (Fig. 3d, compare with Fig. 2b). In the *iGLV6* germinated on estradiol, initiation events consisting of one or two pericycle layers that disproportionately divide anticlinally are predominantly observed, often hindering the quantification of separate initiation events. Consequently, wild-type-looking primordia, as well as ELRs, seldom develop (Fig. 3e,f). In contrast, all LR developmental stages were recognizable in the *iGLV6/mpk6-6* and *iGLV6/mpk6-7* mutants with or without estradiol (Fig. 3d–f). This was confirmed by studying individual initiation events after the induction of LR formation through bending of the primary root. On gravistimulation, a primordium was formed at the outer side of the bend in the mock-treated *iGLV6* line as previously reported[21,22]. When transferred to estradiol a few hours before LR initiation, only anticlinally divided pericycle cells were observed at the bend, similar to the division pattern detected in the *iGLV6* line germinated on estradiol (Extended Data Fig. 2a). Performing the same experiment in the *mpk6-6*, *mpk6-7* and *mpk6-4* backgrounds confirmed the suppression of the *GLV6*^{OE} phenotype by the *mpk6* mutations (Fig. 3g and Extended Data Fig. 2a).

***mpk6* mutants have defects in LR initiation similar to *glv lof* mutants.** The suppression of the *GLV6*^{OE} phenotype during LR initiation points to a function of MPK6 in this process. Indeed, an increase in the total LR density was detected in the *iGLV6/mpk6-6* and *iGLV6/mpk6-7* lines with or without estradiol (Fig. 3f and Supplementary Table 2). Similarly, total LR density was increased in *mpk6-3 and mpk6-4* mutants (Fig. 3f and Supplementary Table 2), confirming earlier published results[19]. The analysis of all primordium stages in *mpk6* mutants revealed a consistent significant increase in non-emerged primordium density, particularly at early stages, with the largest difference found at primordium stages I and II (Fig. 3e,f, Extended Data Fig. 2b and Supplementary Table 2). Taken together, our results indicate increased LR initiation events in *mpk6* mutants, which do not always proceed in development, leading to a strong accumulation of non-emerged primordia. The *mpk6* mutant phenotypes resemble the increase in LR initiation observed in *glv* lines. Interestingly, primordia were also found in close proximity in the *mpk6* mutants (Fig. 3d,h). The corresponding phenotypes of *glv* and *mpk6 lof* mutants in the LR development process point to genes functioning in the same pathway, although the *mpk6* mutant phenotype is stronger. This is probably because MPK6 is a converging point for multiple pathways controlling LR initiation, including but not limited to the GLV pathway.

GLV6p induces MPK6 phosphorylation dependent on RGI receptors. On the basis of our previous results, we postulated that MPK6 conveys phosphorylation events in response to GLV peptides, and we thus tested whether GLV6p treatment induces MPK6 phosphorylation. Using anti-phospho-44/42 antibodies, we detected rapid and transient MPK6 phosphorylation in wild-type seedlings minutes after GLV6p treatment reminiscent of patterns previously reported for other ligands (Fig. 4a,b and Supplementary Fig. 4a,b)[23]. MPK3 was also phosphorylated on the addition of GLV6p, albeit to a lesser degree than MPK6.

Recently, a family of five leucine-rich repeat receptor-like kinases was identified by three independent groups as the receptors for RGF1/GLV11. They were named RGFRs or RGIs (refs. [24–26]) (hereafter referred to as RGI1 to 5). We wondered whether any of the RGI receptors could also serve as receptors for GLV6/10 during the LR initiation process. On the basis of available transcriptomic compendia generated on the induction of LR formation[27,28], *RGI1*, *RGI4* and *RGI5* transcription seems to be activated before stage I, *RGI2* transcription is activated from stage III or IV and *RGI3* is not expressed in LRs (Supplementary Fig. 5a). Because of their early induction, *RGI1*, *RGI4* and *RGI5* are the most likely candidate receptors in the GLV pathway during LR initiation. An analysis of transcriptional reporters revealed *RGI1* expression in all xylem-pole pericycle cells at the beginning of the differentiation zone where no primordia had yet been formed. After primordium formation, *RGI1* expression is mostly present in the cells at the base of the primordia (Fig. 5a). *RGI5* expression appeared in LR founder cells and remained in all

primordium cells after the first ACD. GFP signal also appeared in the endodermal and cortical cells adjacent to the forming primordium. Unfortunately, we could not detect *RGI4* expression in the mature root region, probably owing to very low promoter activity (Supplementary Fig. 5b). To investigate a possible function in LR initiation, we examined two independent *lof* mutant lines for each receptor but could not find differences in LR density compared with the wild type (data not shown). Nevertheless, an increase in the percentage of five- or six-celled stage I primordia, similar to the *glv6 glv10* phenotype, was observed in *rgi1* and *rgi4* but not in *rgi5* mutants (Fig. 5b). Occasionally, stage I primordia with more than six cells were observed in the *rgi* mutants (Fig. 5b). This phenotype points to additional ACD taking place and is in agreement with *RGI1*, but not *RGI5*, expression in the flanks of the forming primordium.

To test whether RGI1, RGI4 and RGI5 act downstream of GLV peptides during LR initiation, we analysed the *GLV6*^{OE} LR phenotype in single and triple *rgi145* mutant backgrounds. The quantification of ELRs revealed a small suppression of the phenotype in single *rgi* mutants compared with the wild type, while almost full suppression was observed in the triple *rgi145* mutant background (Fig. 5c,e and Supplementary Fig. 6a). This suggests that RGI receptors act redundantly downstream of GLV peptides during LR formation. A microscopic analysis showed that the aberrant pericycle divisions induced by an excess of GLV6 were also suppressed in the *rgi145* mutant, and dome-shaped primordia were formed instead (Fig. 5d). Similarly, the increased pericycle anticlinal symmetric divisions and the consequent drop in ELR density induced by GLV10p treatment in the wild type was slightly reduced in *rgi1* and *rgi4* mutants and almost completely suppressed in the *rgi145* mutant (Fig. 5f and Supplementary Fig. 6c,d). The expression of an RGI1–Venus fusion protein driven by the constitutive *RPS5A* promoter restored the small root apical meristem of the *iGLV6/rgi145* mutant without estradiol, but not the root length. This could be the consequence of only partial redundancy in RGI receptors and/or additional defects triggered by overexpressing *RGI1* (Fig. 5c and Supplementary Fig. 6e,f). The wavy root phenotype[12] and the reduction in ELRs caused by *GLV6*^{OE} were also (partially) recovered in the *iGLV6/rgi145/RPS5Apro:RGI1–Venus* line (Fig. 5c,e). Increased anticlinal symmetric pericycle divisions on induction of *GLV6*^{OE} were observed in *iGLV6/rgi145/RPS5Apro:RGI1–Venus* roots, although they were not as continuous as in the wild type (Fig. 5d). These data indicate that RGI receptors are necessary for the LR phenotype induced by GLV excess and that RGI1 can partially compensate for the *rgi145* defects in the GLV pathway.

Finally, we analysed whether RGI receptors are necessary for the MPK6 phosphorylation triggered by GLV6p treatment. Indeed, the GLV6p-induced phosphorylation of MPK6 was highly decreased in the *rgi145* triple mutant, indicating that MPK6 phosphorylation by GLV6p treatment is also dependent on the RGI receptors (Fig. 5g,h and Supplementary Fig. 4c).

GLV and RGI expression are induced by auxin while *GLV6*^{OE} negatively influences auxin accumulation and signalling. Auxin is known to be crucial for LR initiation, as mutants in auxin signalling fail to initiate LRs[29,30]. *GLV6* and *GLV10* expression patterns during LR initiation resemble those of auxin reporters containing the *DR5* promoter (Fig. 1a)[11,31,32]. We therefore tested whether auxin induces *GLV6/10* and *RGI1/4/5* transcription. Indeed, after short treatments with the auxin analogue 1-naphthaleneacetic acid, all transcripts were induced, and this was dependent on *ARF7*, *ARF19* and *IAA14*, which are components of auxin signalling known to be involved in LR initiation (Fig. 6a and Supplementary Fig. 7)[29,30]. We then tested whether *GLV6*^{OE} affected auxin accumulation and/or signalling. We crossed the *iGLV6* line to a *DR5pro:Luciferase* reporter[1] and quantified the *DR5pro:Luciferase* signal during prebranch site formation in mock or estradiol-induced roots. The results show that the *DR5pro:Luciferase* signal decreased on *GLV6*^{OE}, indicating a negative effect of the GLV pathway on auxin accumulation and/or signalling (Fig. 6b–d).

Discussion

Our suppressor screen identified MPK6 as a downstream effector of the GLV pathway during LR initiation. This is in line with previous reports showing that MPK6 acts downstream of peptide signalling in plant developmental processes[33,34]. Although *mpk6* mutants suppressed the *GLV6*^{OE} phenotype to a large degree, MPK3 could act redundantly with MPK6 during LR initiation and contribute to a lesser extent to the GLV pathway. It is very likely that the perception of GLV6 and GLV10 peptides upstream of MPK6 is mediated by the RGI1, RGI4 and RGI5 receptors. Although receptor–ligand binding assays need to be performed to confirm that RGIs are receptors for GLV6/GLV10, it was shown that both peptides can bind to RGI3 with high affinity[24] and that GLV10 competed for the binding of GLV11/RGF1 to RGI1. Unfortunately, we were not able to successfully purify RGI ectodomains from heterologous systems. Like the *glv6 glv10* mutant, the *rgi1* and *rgi4* mutants display increased ACD, indicating that like GLV peptides, RGI1 and RGI4 are necessary to restrict ACD during the first steps of LR formation.

Our data point to GLV peptides acting as inhibitors to prevent an excess of ACDs from taking place after LR founder cell specification. Knocking out *GLV6* and *GLV10* genes resulted in increased LR initiation, indicating that more of the primed LR founder cells undergo the first ACD when GLV levels are low. A second ACD happened more frequently in *glv* mutants than in the wild type as well. Since *GLV6* and *GLV10* are both transcribed in LR founder cells and expression seems stronger in the central cells after the first ACD (Fig. 1a)[12], it is tempting to think that the principles of Turing's reaction–diffusion model resulting in lateral inhibition apply during LR initiation[35]. The Turing mechanism has been used to explain the generation of patterns in living organisms such as the skin stripes in zebrafish and stomata and trichome cell patterning in plants[36]. In the activator–inhibitor model proposed by Turing, the interaction between a self-activator and a diffusing inhibitor generates patterns from undifferentiated cells. In the case of LR initiation, an unknown activator would promote ACD in LR founder cells, while cell-autonomous GLV signalling induced by the activator would counteract that effect. In the event that the first ACD proceeds and LR initiation takes place owing to differences in the levels of activator and inhibitor, GLV6 expression or secretion induced by the activator mainly in central cells (trans-) inhibits flanking cells from undergoing a second ACD (Fig. 6e,f). In the frame of LR initiation, the generation of GLV gradients and the direction of signalling might be important for patterning, as the overexpression of *GLV6* equally in all cell layers results in pericycle cells undergoing symmetric divisions instead of no division at all[12]. As in other biological systems, more complex regulation is probably at play during LR initiation, and the presence of undiscovered factors has to be taken into account. However, on the basis of the current knowledge of LR initiation, we can speculate on a possible scenario. Most probably, auxin acts upstream of both the activator and GLV6 signalling (Fig. 6e). In agreement with this, the transcription of *GLV6, GLV10* and the *RGI1*, *RGI4* and *RGI5* receptors was induced by auxin treatment. Concurring also with our model, the *DR5pro:Luciferase* signal reporting auxin maxima was decreased during prebranch site formation after the induction of *GLV6* overexpression (Fig. 6b–d), indicating a negative feedback of the GLV pathway on auxin accumulation or signalling.

A recent publication points to another signalling peptide that regulates LR spacing. The TARGET OF LBD SIXTEEN 2 (TOLS2)/PAMP-INDUCED SECRETED PEPTIDE-LIKE 3 (PIPL3) peptide transcription is induced in LR founder cells and signals to the

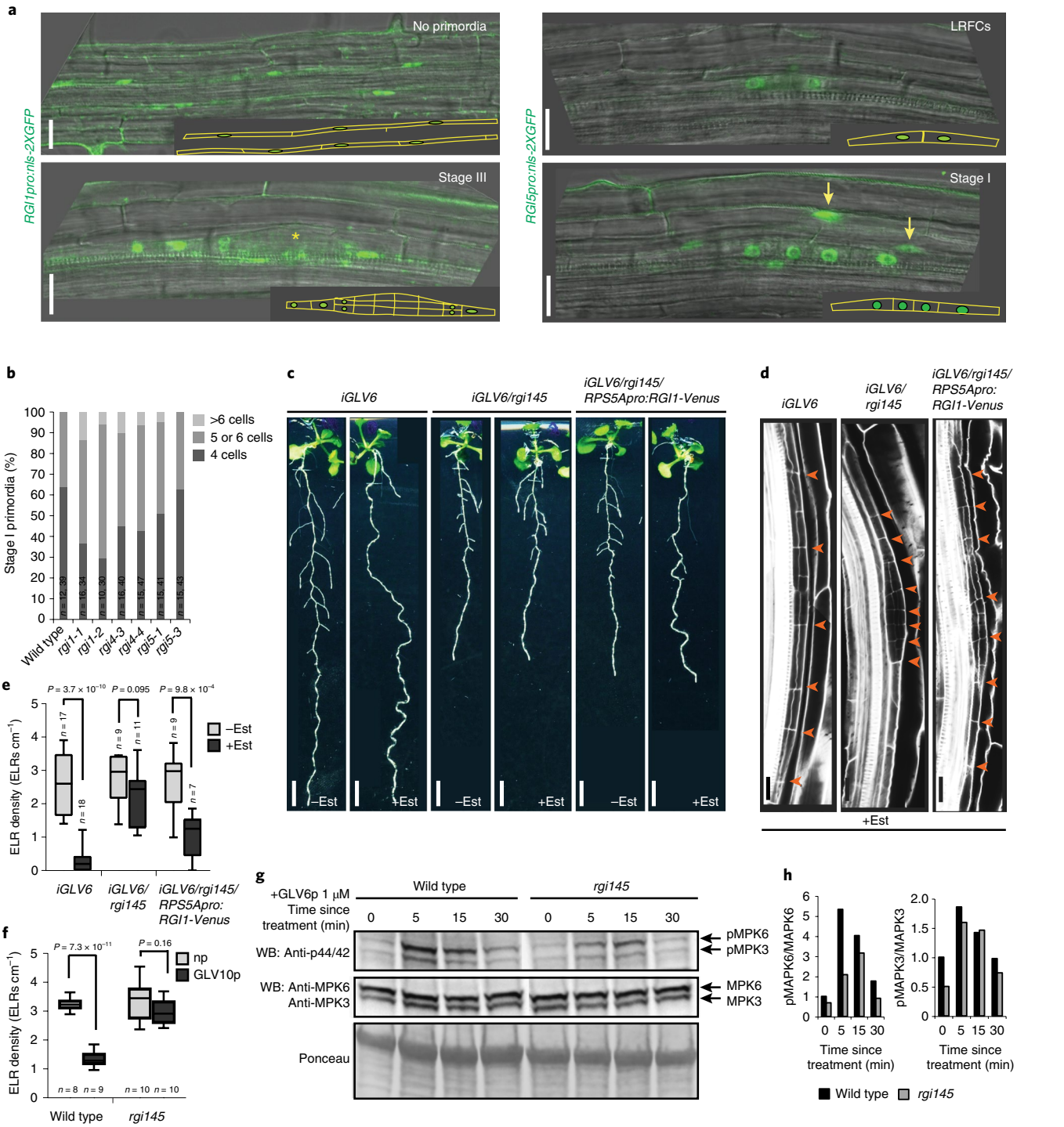

Fig. 5 | *GLV6*^{OE} phenotypes and the induction of MPK6 phosphorylation are dependent on RGI receptors. a, *RGIpro:nls-2XGFP* signal in pericycle cells and during primordium formation. The beginning of the differentiation zone where no primordia have formed yet or where a primordium is developing was imaged. Primordium stages are indicated in the upper right corner. The yellow asterisk indicates a stage III primordium. The arrows indicate GFP signal in endodermal and cortical cells in front of the forming primordium. Inset: schematic representation of *RGI* expression. **b**, Quantification of stage I primordia that have undergone one or two rounds of ACDs. The percentage of four- or five/six-celled stage I primordia in the wild type and the *rgi* mutants (9 dag) is shown (*n*, number of roots, number of primordia). **c**,**d**, Estradiol induction of *GLV6*^{OE} results in decreased ELR density and increased root wavy growth (**c**), and excessive pericycle anticlinal divisions (**d**). These phenotypes are suppressed in the *rgi145* mutant and partially rescued in the *RPS5pro:RGI1:Venus/ rgi145* line. The arrowheads indicate anticlinal divisions across all pericycle layers. **e**, Quantification of ELRs in the *iGLV6/rgi145* mutant and the *iGLV6/ RPS5pro:RGI1:Venus/rgi145* line with and without estradiol compared with the *iGLV6* control (13 dag). **f**, Quantification of ELRs in the *rgi145* mutant compared with the wild type (14 dag) germinated on GLV10p (100 nM). **g**, GLV6p-induced MPK6 phosphorylation is decreased in the *rgi145* triple mutant. **h**, Quantification of the ratio between the phosphorylated MPK6 or MPK3 (pMPK6/3) and the MPK6 or MPK3 protein signal shown in **g**, respectively. The fold change relative to time 0 (wild type) is shown. This experiment was done three times with similar results. Different treatments for the same genotype are compared using a two-sided Student's *t*-test. The scale bars represent 20 µm in **a** and **d** and 0.5 cm in **c**.

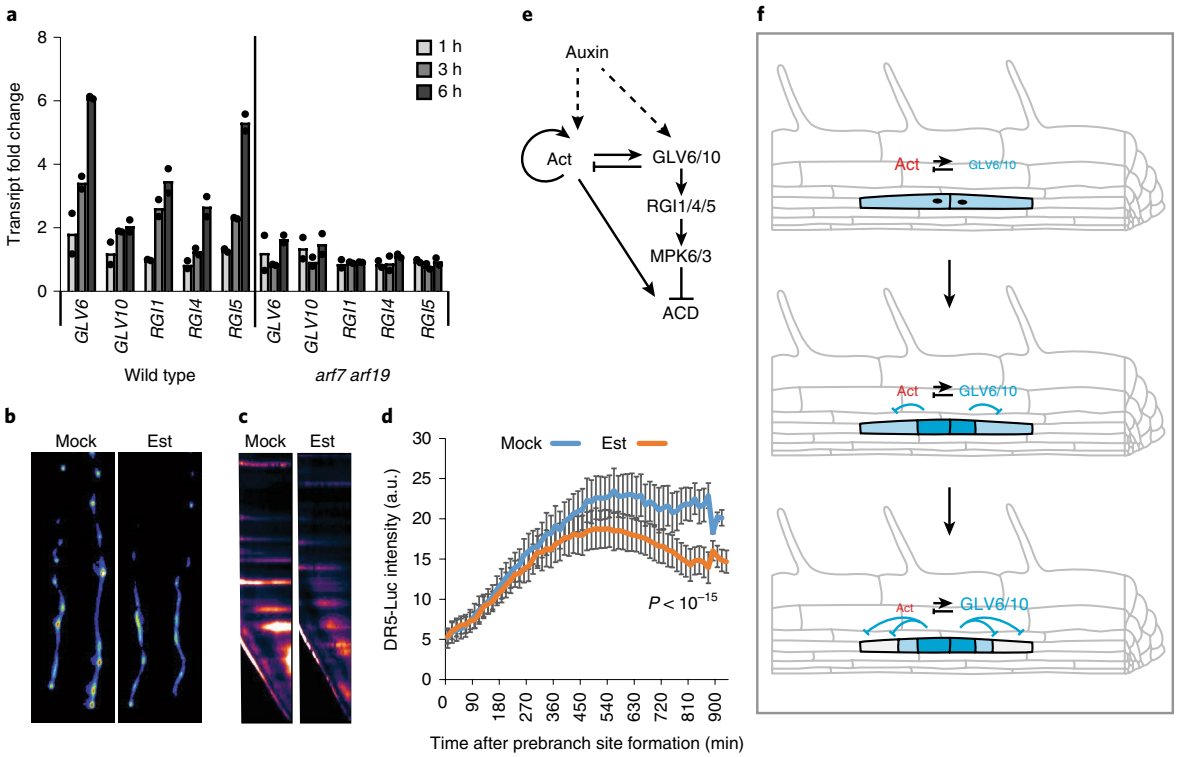

Fig. 6 | Model for GLV6/10 signalling restricting ACD during LR initiation. a, Quantification of *GLV6/10* and *RGI1/4/5* transcript fold change after treatment with 10 µM 1-naphthaleneacetic acid relative to mock treatment for the indicated time points in the wild type and in *arf7 arf19* mutants, detected by quantitative PCR with reverse transcription. The bars show the mean values of two independent replicates. **b**, *iGLV6xDR5pro:Luciferase* seedlings 840 min after transfer to mock or estradiol treatment. **c**, Kymographs showing the *iGLV6xDR5pro:Luciferase* signal of a representative root transferred to mock or estradiol treatment. **d**, Quantification of the *iGLV6xDR5pro:Luciferase* signal in seedlings transferred to mock or estradiol treatment. The graph shows the mean values ± s.e.m ($n = 8$). The time 0 (540–660 min after transfer) was normalized for all roots as the start of a prebranch site. An extra sum-of-squares *F*-test was performed to determine whether one or multiple models could adequately describe the data for all conditions. A single model was not sufficient to describe the two datasets ($P < 10^{-15}$). **e**, GLV6/10 signals through the RGI1, RGI4 and RGI5 receptors and MPK6 to inhibit ACD. Auxin probably acts upstream of GLV signalling, potentially via an activator gene (Act). **f**, LR founder cells have high levels of a self-enhancing activator (Act) of ACD, which, in turn, induces *GLV6/10* transcription in LR founder cells that inhibits ACD and reduces the levels of Act. If the levels of Act are higher than GLV levels, ACD takes place, resulting in GLV6/10 transcription mainly in the central cells. GLV6/10 trans-inhibits ACD in the large flanking daughter cells. If Act levels are still higher than GLV levels, a second ACD takes place in the flanking cells. The induction of GLV6/10 would eventually result in the reduction of the Act levels and the lateral inhibition of ACD. The relative levels of Act and GLV6 are reflected in the text sizes. The blue fill represents GLV6/10 transcription.

cells flanking the nascent primordium through the RLK7 receptor[37]. In contrast, we found that *RGI* receptors are transcribed in all xylem-pole pericycle cells (*RGI1*) or in LR founder cells (*RGI5*) where LRs initiate. Therefore, the TOLS2/PIPL3-RLK7 pathway could be activated downstream or concomitantly with GLV6/10 signalling to spatially propagate lateral inhibition to the cells flanking the LR founder cells after they have been specified. It is fascinating that plants may deploy different signalling peptides to guarantee the correct LR formation and patterning. Different signalling peptide pathways probably contribute to LR formation at different stages, as it has been shown for the IDA peptide and its receptors, necessary for the separation of outer root cell layers during LR emergence[38]. Remarkably, this IDA-HAE/HSL2-dependent cell separation also involves the activation of MPK3 and MPK6 (ref. [39]). How different signalling peptides that use a common downstream component result in specific developmental outputs is a challenging but essential question that needs to be addressed in future studies to understand how signalling pathways operate during plant development.

Methods

Plant material and growth conditions. The seedlings were sown on solid half MS medium (Duchefa Biochemie B.V.) supplemented with 1% sucrose (VWR), 0.1 g l^{-1} Myo-inositol (Sigma-Aldrich), 0.5 g l^{-1} MES (Duchefa Biochemie B.V.) and 0.8% Plant Agar (Lab M, MC029). The plates were stratified for 2 d at 4 °C and grown at 21 °C under continuous light conditions. For the phenotypic analysis, the seedlings were germinated on mock (dimethylsulfoxide (DMSO)) or 2 µM estradiol unless otherwise specified.

The *iGLV6* line was generated by Gateway LR recombination reaction using the *pEN-L1-GLV6-L2* (ref. [11]) and the estradiol-inducible pMDC7_B(pUBQ) vector[40,41]. To generate the *glv6* CRISPR–Cas mutants, three guide RNAs were designed targeting the first and fourth exons of the *GLV6* gene (Supplementary Table 1 and Supplementary Methods). The sextuple *glv* mutant was also generated by CRISPR–Cas9 (ref. [13]). This mutant was originally intended to knockout *GLV* genes transcribed in aerial tissues, and therefore *GLV1*, *GLV2*, *GLV6*, *GLV7*, *GLV8* and *GLV10* were targeted. The *CLE18* gene, encoding a precursor that contains a GLV motif in the carboxy terminus[10], was also mutated. Out of the six targeted *GLV* genes, only *GLV6* and *GLV10* were found to be transcribed early during LR initiation. *GLV7* is transcribed from stage IV primordia onwards, *GLV2* and *GLV8* are transcribed only in ELRs, and *GLV1* is not expressed at all in the root[11]. *CLE18* expression has been reported in the primary root pericycle and vascular tissues of mature LRs (ref. [42]); however, we could not confirm *CLE18* transcription in the primary root tissues after RNA-Seq experiments were performed in root segments of the young maturation zone (J.J. et al., unpublished results; Chen et al., unpublished results).

The *glv6 glv10* double mutant was obtained by crossing a *glv10* tDNA insertion mutant (*Salk_048797*) with the *CRISPR glv6-2* line. The mutant lines were validated by quantitative or non-quantitative PCR with reverse transcription (Supplementary Fig. 8a–c and Supplementary Methods).

***iGLV6* EMS mutagenesis and mutation identification.** A total of 8,000 *iGLV6*^{OE} seeds were incubated for 5 min in 0.1 M phosphate buffer (pH = 7.5) containing 0.05% Triton X-100. After washing with water, the seeds were incubated for 7 h in 0.3% EMS in phosphate buffer (v:v) (final concentration, 30 mM). The seeds were washed with $Na_2S_2O_3$ five times, then eight times with water. The M1 seeds were planted on soil in pools of 50–70 plants each. The M2 population from each pool was harvested and screened (60,000 M2 seeds in total) on MS plates containing 2 µM estradiol for the presence of seedlings with ELRs. Mutants showing suppression of the *GLV6*^{OE} LR phenotype were transferred to soil, and the phenotype was confirmed in the M3. Fifteen mutants totally or partially suppressing the *GLV6*^{OE} ELR phenotype were confirmed in the M3. Of those, eight resulted in decreased *GLV6* overexpression levels and one in a stop codon in the *GLV6* coding sequence present in the transgene; these mutants were thus discarded. We also excluded one mutant with a limited suppression of the *GLV6*^{OE} phenotype and exhibiting strong developmental defects. We ended up with five confirmed *sgps*.

The *TPST* gene was PCR-amplified and sequenced in *sgp1* and *sgp2*. For next-generation sequencing, *sgp3* and *sgp4* were back-crossed to the unmutagenized *iGLV6* line, and seedlings showing suppression of the *GLV6*^{OE} phenotype were selected and pooled from the F2 segregating population. Nuclear DNA was isolated from 40–80 pooled seedlings. Next-generation sequencing was performed with the Illumina Hi Seq 2500 platform (Eurofins) using paired-end sequencing and 36-fold genome coverage. The mutations were mapped with SHOREmap[43] (v.2.0) using the *A. thaliana* genome as a reference (TAIR10). The *iGLV6* parental line was not sequenced. The mutations that were found in all mutants were probably already present in the *iGLV6* line and were thus discarded. Nine and three non-synonymous candidate suppressive mutations were obtained for *sgp3* and *sgp4*, respectively (Supplementary Fig. 9). The only gene mutated in both lines was *MPK6*. Because *sgp3* and *sgp4* are allelic in suppressing the *GLV6*^{OE} phenotype (Supplementary Fig. 1e), we reasoned that the mutations found in *MPK6* must be responsible for the suppression of the *GLV6*^{OE} phenotype.

The *sgp5* mutant was also studied using next-generation sequencing. This mutant carries two candidate suppressive mutations in the *AT2G06050* and *AT2G22360* genes encoding for the OXOPHYTODIENOATE-REDUCTASE 3 (OPR3) involved in jasmonate biosynthesis, and the DNA J PROTEIN A6, respectively. Both mutations in *sgp5* generate a P to L change. It is not clear which of these is the suppressive mutation.

Light microscopy. When only ELRs were quantified, the analysis was performed in 12–14 dag seedlings grown on solid MS (except for the GLV6p treatment assays) using a binocular microscope (Leica). The root lengths were measured with ImageJ[44,45] (v.1.50e). The LR density was calculated by dividing the LR number by the primary root length.

For the analysis of all LR developmental stages, 8–9 dag seedlings were collected and cleared using a modified Malamy and Benfey[46] protocol (Supplementary Methods). All LR stages including primordia and ELRs were counted using an Olympus BX53 DIC microscope with a ×400 magnification. Under our growth conditions, the average distance between two primordia or LRs was 0.97 ± 0.24 mm (mean ± s.e.m., $n = 5$ roots, 22–28 primordia per root) in the wild type. Nearby primordia or LRs were counted if they could be observed together in the microscope view field using the ×40 objective (distance between primordia equal to or less than 0.5 mm). The pictures were taken with an Olympus BX53 DIC microscope or a VHX-7000 digital microscope (KEYENCE) equipped with a fully integrated head.

The *mpk6* pleiotropic root phenotypes were classified according to Lopez-Bucio[19] (Supplementary Fig. 3b). The *mpk6lr* roots were used for the quantification of non-emerged primordia and ELRs.

For the induction of LR primordia after primary root bending, 3 dag seedlings grown vertically on solid MS were gravistimulated for 6 h, then transferred to mock or estradiol treatment for 44 h. The seedlings were then mounted on chloral hydrate, and the numbers and stages of primordia formed at the bend were scored under an Olympus BX53 DIC microscope.

Peptide treatments. The GLV6p: DY(SO_3)RTFRRRRPVHN and rGLV6p: NRRY(SO_3)RHRFTVDPR were synthesized as previously described[17]. The GLV10p: DY(SO_3)PKPSTRPPRHN was ordered from GenScript. For ELR counting, the seedlings were germinated in liquid MS containing 2 µM GLV6p for 7 d, then fixed with 90% acetone, washed once with PBS buffer and finally mounted in lactic acid before ELR quantification under a binocular microscope. For mutant phenotype rescue, the seedlings were grown on solid MS containing the GLV6p or GLV10p at the indicated concentrations.

Protein extraction and western blotting. Wild-type or mutant seedlings were germinated on solid half MS medium for 4 d. Then, 20–40 seedlings were transferred to multiwell plates containing 3 ml of liquid half MS. After 1 h of conditioning, the medium was supplemented with 1 µM GLV6p or rGLV6p, and the seedlings were incubated with the peptides for the indicated times, after which they were harvested and frozen in liquid N_2. Alternatively, the seedlings were germinated in liquid half MS medium. The peptides were then added to the medium, and the seedlings were incubated for the indicated times before sampling. Both methods yielded similar outcomes (Supplementary Fig. 4a,b).

To detect MPK6/3 phosphorylation, an anti-phospho-p44/42 (Cell Signaling Technology; 1:2,500) antibody was used. After stripping, the membranes were reblotted with anti-MPK6 antibody (Sigma-Aldrich; 1:8,000) and anti-MPK3 antibody (Sigma-Aldrich; 1:2,500). All blots were imaged in a ChemiDoc XRS+ imaging system (Biorad). For the quantification of the relative pMPK6 or pMPK3 signal, the band intensity was measured with ImageLab software (v.6.0.0, Bio-rad) and then divided by the MPK6 or MPK3 signal, respectively, for every time point. Afterwards, the values were normalized by the time 0 values.

We need to point out that because MPK6/3 signalling can also be activated by wounding (L.A.N.C. et al., unpublished results), we were not able to detect MPK6 phosphorylation induced by GLV6p specifically in root tissues. Therefore, the GLV6p activation of MPK6/3 reported here includes shoot-derived as well as root-derived responses where *GLV* and *RGI* genes are also transcribed[11,24].

***DR5pro:Luciferase* imaging and quantification.** The *iGLV6* line was crossed to the *DR5pro:Luciferase* (ref. [1]), and 5 dag double homozygous seedlings were transferred to mock (DMSO) or estradiol (2 µM) treatment. The seedlings were sprayed with D-Luciferin (Duchefa; 1 mM D-Luciferin, 0.1% DMSO, 0.01% Tween-80) and kept in the growth room for 3 h to induce *GLV6* expression. The seedlings were then imaged every 15 min with an exposure time of 10 min in a NightShade in vivo plant imaging system (Berthold). ImageJ was used for signal quantification as previously described[47]. After the oscilation signal, the time with the lowest signal was considered time 0 (540–660 min after transfer to treatment) and was normalized for all seedlings as the start of a prebranch site.

Statistical analysis. A two-sided Student's *t*-test was used for the comparison of two conditions or genotypes. The comparison of root lengths between multiple genotypes was performed by one-way analysis of variance. Other statistical analyses were performed in SAS (version 9.4 of the SAS System for Windows). For the analysis of different LR developmental stages, a GEE model was fitted to the primordium count rate with the genotype and developmental stage, as well as the interaction, as fixed effects using a log link function and selecting a Poisson distribution. The log-transformed root length was used as an offset. The correlations between the counts were modelled as exchangeable correlations. At each stage, we tested whether there was an equal primordium count rate in the mutant compared with the wild type, and if applicable, whether there was an equal primordium count rate between the mutant complemented with the peptide and the mutant without the peptide. The analysis was done with the genmod procedure. Contrast statements were set up with the plm procedure using the lsmestimate statement. A significance level of 0.05 was chosen. To correct for multiple testing, the maxT procedure was used as implemented in the plm procedure. The data on non-emerged, emerged and total LR densities as well as the data on clustered LR primordia were analysed by fitting a generalized linear model to the LR counts with the experimental condition (genotype and treatment) as a fixed effect, or if applicable, with the genotype and treatment as well as the interaction term as fixed effects. A Poisson distribution was chosen, except when overdispersion was suspected, in which case we used a negative binomial distribution. A log link function was applied, and log-transformed root length was used as an offset. Contrasts were set up with the plm procedure using the lsmeans statement. A significance level of 0.05 was chosen. To correct for multiple testing, a Tuckey correction was applied. All statistical tests used are two-sided.

For the comparison of *DR5pro:Luciferase* between mock and estradiol treatments, second-order polynomial models were fitted to the data via least squares regression using GraphPad Prism (v.8.0.1 for Windows, GraphPad Software; www.graphpad.com). An extra sum-of-squares *F*-test was performed to determine whether one or multiple models could adequately describe the data for all conditions. A single model was not sufficient to describe the two datasets ($P < 10^{-15}$).

Reporting Summary. Further information on research design is available in the Nature Research Reporting Summary linked to this article.

Data availability

The data supporting the findings in this study are available from the corresponding author upon reasonable request.

Received: 1 April 2019; Accepted: 24 March 2020;
Published online: 11 May 2020

References

1. Moreno-Risueno, M. A. et al. Oscillating gene expression determines competence for periodic *Arabidopsis* root branching. *Science* **329**, 1306–1311 (2010).
2. Xuan, W. et al. Cyclic programmed cell death stimulates hormone signaling and root development in *Arabidopsis*. *Science* **351**, 384–387 (2016).
3. De Smet, I. et al. Receptor-like kinase ACR4 restricts formative cell divisions in the *Arabidopsis* root. *Science* **322**, 594–597 (2008).

4. De Smet, I. et al. Bimodular auxin response controls organogenesis in *Arabidopsis*. *Proc. Natl Acad. Sci. USA* **107**, 2705–2710 (2010).
5. De Rybel, B. et al. A novel aux/IAA28 signaling cascade activates GATA23-dependent specification of lateral root founder cell identity. *Curr. Biol.* **20**, 1697–1706 (2010).
6. Hofhuis, H. et al. Phyllotaxis and rhizotaxis in *Arabidopsis* are modified by three PLETHORA transcription factors. *Curr. Biol.* **23**, 956–962 (2013).
7. Casimiro, I. et al. Auxin transport promotes *Arabidopsis* lateral root initiation. *Plant Cell* **13**, 843–852 (2001).
8. Lucas, M. et al. Lateral root morphogenesis is dependent on the mechanical properties of the overlaying tissues. *Proc. Natl Acad. Sci. USA* **110**, 5229–5234 (2013).
9. von Wangenheim, D. et al. Rules and self-organizing properties of post-embryonic plant organ cell division patterns. *Curr. Biol.* **26**, 439–449 (2016).
10. Meng, L., Buchanan, B. B., Feldman, L. J. & Luan, S. CLE-like (CLEL) peptides control the pattern of root growth and lateral root development in *Arabidopsis*. *Proc. Natl Acad. Sci. USA* **109**, 1760–1765 (2012).
11. Fernandez, A. et al. Transcriptional and functional classification of the GOLVEN/ROOT GROWTH FACTOR/CLE-like signaling peptides reveals their role in lateral root and hair formation. *Plant Physiol.* **161**, 954–970 (2013).
12. Fernandez, A. et al. The GLV6/RGF8/CLEL2 peptide regulates early pericycle divisions during lateral root initiation. *J. Exp. Bot.* **66**, 5245–5256 (2015).
13. Peterson, B. A. et al. Genome-wide assessment of efficiency and specificity in CRISPR/Cas9 mediated multiple site targeting in *Arabidopsis*. *PLoS ONE* **11**, e0162169 (2016).
14. Komori, R., Amano, Y., Ogawa-Ohnishi, M. & Matsubayashi, Y. Identification of tyrosylprotein sulfotransferase in *Arabidopsis*. *Proc. Natl Acad. Sci. USA* **106**, 15067–15072 (2009).
15. Zhou, W. et al. *Arabidopsis* tyrosylprotein sulfotransferase acts in the auxin/PLETHORA pathway in regulating postembryonic maintenance of the root stem cell niche. *Plant Cell* **22**, 3692–3709 (2010).
16. Matsuzaki, Y., Ogawa-Ohnishi, M., Mori, A. & Matsubayashi, Y. Secreted peptide signals required for maintenance of root stem cell niche in *Arabidopsis*. *Science* **329**, 1065–1067 (2010).
17. Whitford, R. et al. GOLVEN secretory peptides regulate auxin carrier turnover during plant gravitropic responses. *Dev. Cell* **22**, 678–685 (2012).
18. Wu, T. et al. An *Arabidopsis thaliana* copper-sensitive mutant suggests a role of phytosulfokine in ethylene production. *J. Exp. Bot.* **66**, 3657–3667 (2015).
19. Lopez-Bucio, J. S. et al. *Arabidopsis thaliana* mitogen-activated protein kinase 6 is involved in seed formation and modulation of primary and lateral root development. *J. Exp. Bot.* **65**, 169–183 (2014).
20. Xu, J. & Zhang, S. Mitogen-activated protein kinase cascades in signaling plant growth and development. *Trends Plant Sci.* **20**, 56–64 (2015).
21. Ditengou, F. A. et al. Mechanical induction of lateral root initiation in *Arabidopsis thaliana*. *Proc. Natl Acad. Sci. USA* **105**, 18818–18823 (2008).
22. Laskowski, M. et al. Root system architecture from coupling cell shape to auxin transport. *PLoS Biol.* **6**, e307 (2008).
23. Ortiz-Morea, F. A. et al. Danger-associated peptide signaling in *Arabidopsis* requires clathrin. *Proc. Natl Acad. Sci. USA* **113**, 11028–11033 (2016).
24. Song, W. et al. Signature motif-guided identification of receptors for peptide hormones essential for root meristem growth. *Cell Res.* **26**, 674–685 (2016).
25. Ou, Y. et al. RGF1 INSENSITIVE 1 to 5, a group of LRR receptor-like kinases, are essential for the perception of root meristem growth factor 1 in *Arabidopsis thaliana*. *Cell Res.* **26**, 686–698 (2016).
26. Shinohara, H., Mori, A., Yasue, N., Sumida, K. & Matsubayashi, Y. Identification of three LRR-RKs involved in perception of root meristem growth factor in *Arabidopsis*. *Proc. Natl Acad. Sci. USA* **113**, 3897–3902 (2016).
27. Voss, U. et al. The circadian clock rephases during lateral root organ initiation in *Arabidopsis thaliana*. *Nat. Commun.* **6**, 7641 (2015).
28. Peret, B. et al. Auxin regulates aquaporin function to facilitate lateral root emergence. *Nat. Cell Biol.* **14**, 991–998 (2012).
29. Fukaki, H., Tameda, S., Masuda, H. & Tasaka, M. Lateral root formation is blocked by a gain-of-function mutation in the SOLITARY-ROOT/IAA14 gene of *Arabidopsis*. *Plant J.* **29**, 153–168 (2002).
30. Okushima, Y. et al. Functional genomic analysis of the AUXIN RESPONSE FACTOR gene family members in *Arabidopsis thaliana*: unique and overlapping functions of ARF7 and ARF19. *Plant Cell* **17**, 444–463 (2005).
31. Benkova, E. et al. Local, efflux-dependent auxin gradients as a common module for plant organ formation. *Cell* **115**, 591–602 (2003).
32. Dubrovsky, J. G. et al. Auxin acts as a local morphogenetic trigger to specify lateral root founder cells. *Proc. Natl Acad. Sci. USA* **105**, 8790–8794 (2008).
33. Cho, S. K. et al. Regulation of floral organ abscission in *Arabidopsis thaliana*. *Proc. Natl Acad. Sci. USA* **105**, 15629–15634 (2008).
34. Jewaria, P. K. et al. Differential effects of the peptides Stomagen, EPF1 and EPF2 on activation of MAP kinase MPK6 and the SPCH protein level. *Plant Cell Physiol.* **54**, 1253–1262 (2013).
35. Turing, A. M. The chemical basis of morphogenesis. *Phil. Trans. R. Soc. Lond. B* **237**, 37–72 (1952).
36. Torii, K. U. Two-dimensional spatial patterning in developmental systems. *Trends Cell Biol.* **22**, 438–446 (2012).
37. Toyokura, K. et al. Lateral inhibition by a peptide hormone–receptor cascade during *Arabidopsis* lateral root founder cell formation. *Dev. Cell* **48**, 64–75 (2019).
38. Kumpf, R. P. et al. Floral organ abscission peptide IDA and its HAE/HSL2 receptors control cell separation during lateral root emergence. *Proc. Natl Acad. Sci. USA* **110**, 5235–5240 (2013).
39. Zhu, Q. et al. A MAPK cascade downstream of IDA-HAE/HSL2 ligand–receptor pair in lateral root emergence. *Nat. Plants* **5**, 414–423 (2019).
40. Curtis, M. D. & Grossniklaus, U. A gateway cloning vector set for high-throughput functional analysis of genes in planta. *Plant Physiol.* **133**, 462–469 (2003).
41. Barbez, E. et al. A novel putative auxin carrier family regulates intracellular auxin homeostasis in plants. *Nature* **485**, 119–122 (2012).
42. Jun, J. et al. Comprehensive analysis of CLE polypeptide signaling gene expression and overexpression activity in *Arabidopsis*. *Plant Physiol.* **154**, 1721–1736 (2010).
43. Schneeberger, K. et al. SHOREmap: simultaneous mapping and mutation identification by deep sequencing. *Nat. Methods* **6**, 550–551 (2009).
44. Schneider, C. A., Rasband, W. S. & Eliceiri, K. W. NIH Image to ImageJ: 25 years of image analysis. *Nat. Methods* **9**, 671–675 (2012).
45. Schindelin, J., Arganda-Carreras, I. & Frise, E. et al. Fiji: an open-source platform for biological-image analysis. *Nat. Methods* **9**, 676–682 (2012).
46. Malamy, J. E. & Benfey, P. N. Organization and cell differentiation in lateral roots of *Arabidopsis thaliana*. *Development* **124**, 33–44 (1997).
47. Xuan, W., Opdenacker, D., Vanneste, S. & Beeckman, T. Long-term in vivo imaging of luciferase-based reporter gene expression in *Arabidopsis* roots. *Methods Mol. Biol.* **1761**, 177–190 (2018).

Acknowledgements

This research was supported by FWO postdoctoral (A.F., grant no. 1293817N) and doctoral (J.J., grant no. 1168218N) fellowships, a China Scholarship Council grant (K.X., no. 201606350134) and a National Science Foundation Plant Genome Research Program Grant (Z.L.N., no. PGRP-1841917). We thank M. Njo for help with preparing the figures, V. Storme for guidance and assistance with the statistical analysis and D. Savatin for training with the MPK6 phosphorylation experiments.

Author contributions

A.I.F. designed the project. A.I.F. generated the *iGLV6* line, performed the EMS mutagenesis screen and analysed the EMS mutants' identity with help from N.V., A.D., D.O. and T.M. A.I.F. and K.X. phenotypically characterized the *CRISPR glv* mutants, and generated and characterized the *rgi* mutants and reporter lines. N.V. generated and characterized the *CRISPR glv6* mutants. N.V., K.X., J.J. and S.M.-H. phenotypically characterized the *mpk6* mutants. J.J., S.M.-H. and H.D.G. characterized the cross-talk between the auxin and GLV pathways. Q.Y. generated the *RGI4* reporter line. B. Parizot performed the in silico expression analysis. L.A.N.C., N.V. and E.R. performed the MPK6 phosphorylation experiments. B. Peterson and Z.L.N. generated the *CRISPR glv* mutants. K.H., W.V. and A.M. synthesized the peptides. J.J. and A.I.F. performed the statistical analysis. A.I.F., N.V. and T.B. wrote the manuscript with input from all authors. T.B. provided guidance and advice on the project, the experiments and the analysis of the results.

Competing interests

The authors declare no competing interests.

Additional information

Extended data is available for this paper at https://doi.org/10.1038/s41477-020-0645-z.

Supplementary information is available for this paper at https://doi.org/10.1038/s41477-020-0645-z.

Correspondence and requests for materials should be addressed to T.B.

Peer review information *Nature Plants* thanks Melinka Butenko, Juan Xu and the other, anonymous, reviewer(s) for their contribution to the peer review of this work.

Reprints and permissions information is available at www.nature.com/reprints.

Publisher's note Springer Nature remains neutral with regard to jurisdictional claims in published maps and institutional affiliations.

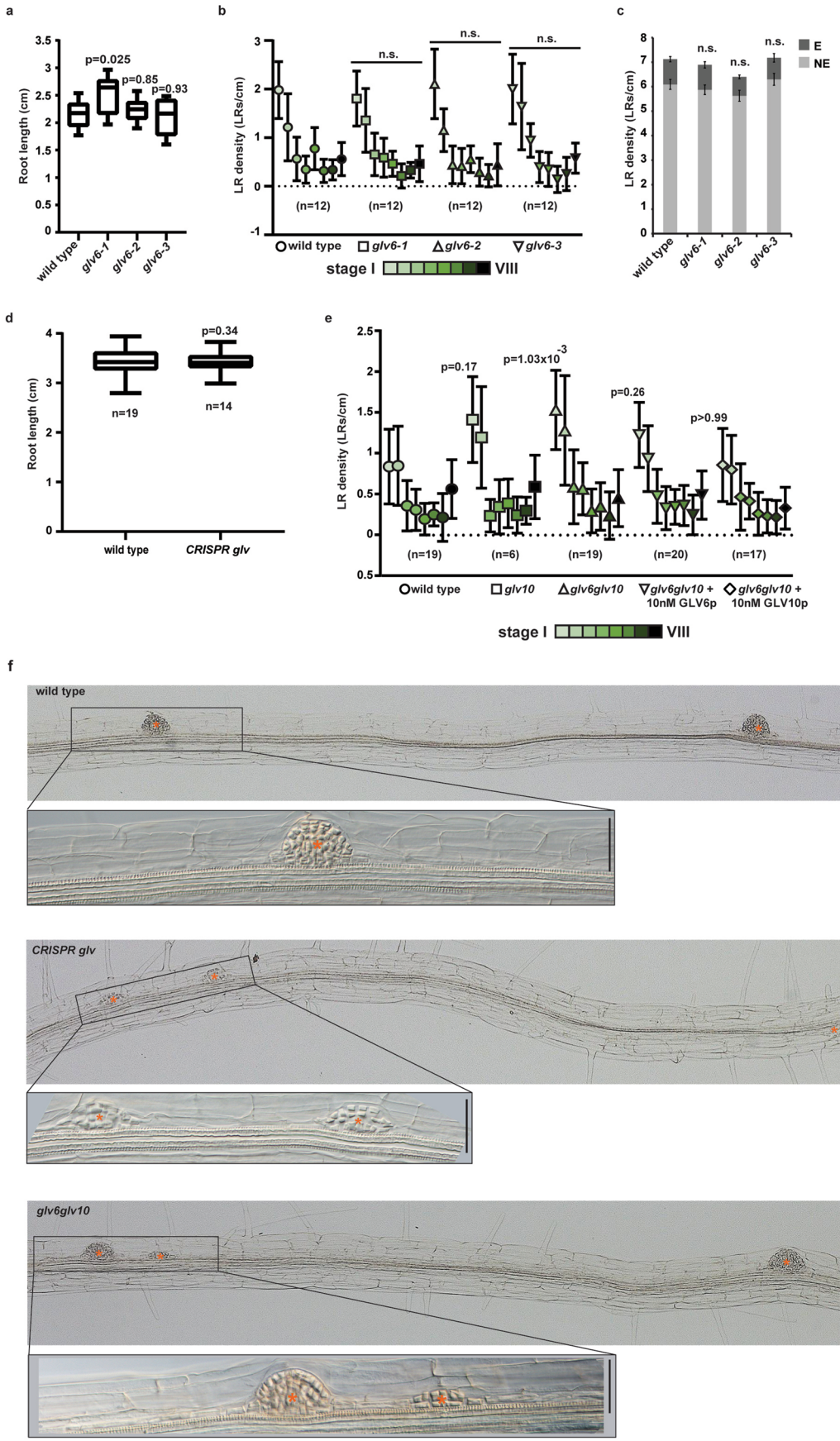

Extended Data Fig. 1 | See next page for caption.

Extended Data Fig. 1 | GLV6 and 10 act redundantly during LR initiation. a–c, Phenotypic characterization of *CRISPR glv6* mutants compared to wild type (8 dag, n = 12). Quantification of root length (a), all primordium stages density (**b**) and non-emerged primordia (NE) and emerged (E) LR density (**c**). **d**, Quantification of root length in the *CRISPR glv* mutant compared to wild type. **e**, Quantification of all primordium stages density in the *glv6glv10* mutant germinated on MS or on 10 nM of GLV6p/GLV10p (8 dag). Charts show mean values ± s.d. (**b**, **e**) or s.e.m (**c**). Significant differences compared to wild type are shown and were determined using one-way ANOVA (**a**, **d**) or a GEE model (**b**-**c**, **e**). In **e**, only significant differences in stage I primordia are displayed. For full statistical analysis see Supplementary Table 2. n.s.: no significant differences were found between mutants and wild type. **f**, Example of nearby primordia frequently found in *glv* mutants. The lower picture shows a higher magnification image of the framed area in the upper picture for each genotype. Scale bars represent 50 µm.

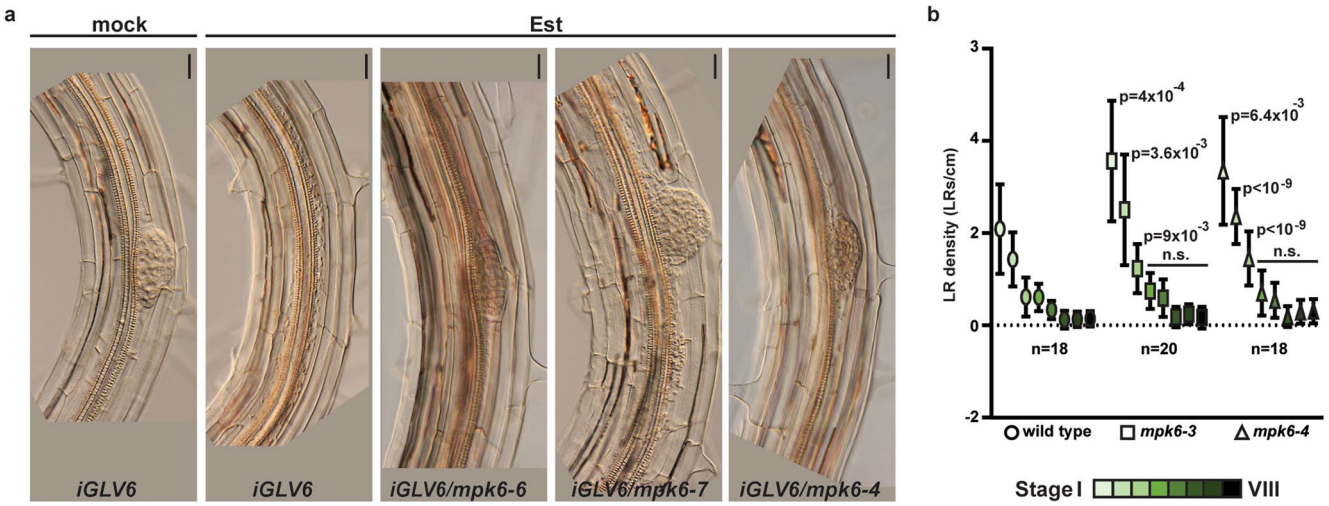

Extended Data Fig. 2 | Suppression of the *GLV6*^{OE} phenotype and LR defects in *mpk6* mutants. a, Suppression of the *GLV6*^{OE} phenotype in *mpk6* mutants after LR initiation was induced by gravistimulation of the primary root. This experiment was done three times with similar results. **b**, Quantification of all primordium stages in reported *mpk6* mutants compared to wild type (8 dag). Chart represents mean values ± s.d. A GEE model was used. n.s.: no significant differences were found between mutants and wild type. For full statistical analysis see Supplementary Table 2. Scale bars represent 20 µm.

nature research

Corresponding author(s): Tom Beeckman

Last updated by author(s): Mar 12, 2020

Reporting Summary

Nature Research wishes to improve the reproducibility of the work that we publish. This form provides structure for consistency and transparency in reporting. For further information on Nature Research policies, see Authors & Referees and the Editorial Policy Checklist.

Statistics

For all statistical analyses, confirm that the following items are present in the figure legend, table legend, main text, or Methods section.

n/a	Confirmed	
☐	☒	The exact sample size (*n*) for each experimental group/condition, given as a discrete number and unit of measurement
☐	☒	A statement on whether measurements were taken from distinct samples or whether the same sample was measured repeatedly
☐	☒	The statistical test(s) used AND whether they are one- or two-sided *Only common tests should be described solely by name; describe more complex techniques in the Methods section.*
☐	☒	A description of all covariates tested
☐	☒	A description of any assumptions or corrections, such as tests of normality and adjustment for multiple comparisons
☐	☒	A full description of the statistical parameters including central tendency (e.g. means) or other basic estimates (e.g. regression coefficient) AND variation (e.g. standard deviation) or associated estimates of uncertainty (e.g. confidence intervals)
☐	☒	For null hypothesis testing, the test statistic (e.g. *F*, *t*, *r*) with confidence intervals, effect sizes, degrees of freedom and *P* value noted *Give P values as exact values whenever suitable.*
☒	☐	For Bayesian analysis, information on the choice of priors and Markov chain Monte Carlo settings
☒	☐	For hierarchical and complex designs, identification of the appropriate level for tests and full reporting of outcomes
☒	☐	Estimates of effect sizes (e.g. Cohen's *d*, Pearson's *r*), indicating how they were calculated

Our web collection on statistics for biologists contains articles on many of the points above.

Software and code

Policy information about availability of computer code

Data collection	No software was used to collect the data
Data analysis	Root length was quantified with ImageJ 1.50e. Band intensity in Western blots was analyzed using the ImageLab software (version 6.0.0, Biorad). Statistical analysis was performed in SAS (Version 9.4 of the SAS System for windows7 64bit). For One-way ANOVA, GraphPad Prism 8.0.1 was used

For manuscripts utilizing custom algorithms or software that are central to the research but not yet described in published literature, software must be made available to editors/reviewers. We strongly encourage code deposition in a community repository (e.g. GitHub). See the Nature Research guidelines for submitting code & software for further information.

Data

Policy information about availability of data

All manuscripts must include a data availability statement. This statement should provide the following information, where applicable:

- Accession codes, unique identifiers, or web links for publicly available datasets
- A list of figures that have associated raw data
- A description of any restrictions on data availability

The data supporting the findings in this study are available from the corresponding author upon reasonable request.

Field-specific reporting

Please select the one below that is the best fit for your research. If you are not sure, read the appropriate sections before making your selection.

☒ Life sciences ☐ Behavioural & social sciences ☐ Ecological, evolutionary & environmental sciences

For a reference copy of the document with all sections, see nature.com/documents/nr-reporting-summary-flat.pdf

Life sciences study design

All studies must disclose on these points even when the disclosure is negative.

Sample size	Determination of sample size is done according to an in-house protocol based on the longstanding experience within the group and on the conventional sample sizes used in the root developmental biology community. In brief, for general comparisons of root parameters (root length, lateral root density) a sample size of 15-20 plants per genotype is aimed at. In the case of peptide treatments, the volume of the growth medium is limiting because of the availability of the peptides and the financial implications when working with larger volumes. In such cases smaller petri-dishes have to be used to decrease the volume of growth media and a smaller number of plants can be followed but a sample size of 10 plants per treatment is intended. Using these samples sizes we observe consistent results indicating that they are representative of the population.
Data exclusions	no data was excluded
Replication	All experiments were repeated, often by independent researchers, with similar outcome.
Randomization	The population we are using (plants) and the kind of experiments (phenotyping mutants and wildtype) is not subjected to intrinsic bias requiring ramdomization to overcome it.
Blinding	Researchers were not blinded during the experiments. Gain- and loss-of-function approaches used in this study generate obvious phenotypes (e.g. GOLVEN phenotype). Blinding will not be very effective in this case.

Reporting for specific materials, systems and methods

We require information from authors about some types of materials, experimental systems and methods used in many studies. Here, indicate whether each material, system or method listed is relevant to your study. If you are not sure if a list item applies to your research, read the appropriate section before selecting a response.

Materials & experimental systems

n/a	Involved in the study
☐	☒ Antibodies
☒	☐ Eukaryotic cell lines
☒	☐ Palaeontology
☒	☐ Animals and other organisms
☒	☐ Human research participants
☒	☐ Clinical data

Methods

n/a	Involved in the study
☒	☐ ChIP-seq
☒	☐ Flow cytometry
☒	☐ MRI-based neuroimaging

Antibodies

Antibodies used	anti-MPK6 antibody (Sigma-Aldrich, Cat# A7104, Lot# 025M4793V); anti-MPK3 (Sigma-Aldrich,Cat# M8318, Lot# 088M4891V); anti-phospho-p44/42 (T202/Y204)(Cell Signaling Technology, Cat# 9101S, Lot: 30)
Validation	These antibodies have been used in previous reports to monitor MPK6/3 phosphorylation. Anti-MPK6: Guo et al., Nat Commun., 2016; anti-MPK3 and anti-phospho-p44/42 (T202/Y204): Sardar et al., JXB, 2017. All antibodies: Ortiz-Morea et al., PNAS 2016. Additional references and validation of the antibodies can be found on the supplier's web page.